Ceramics International 44 (2018) 11658–11664

Contents lists available at ScienceDirect

Ceramics International

journal homepage: www.elsevier.com/locate/ceramint

Modified electrical properties of chemical solution deposited epitaxial $BiFeO_3$ thin films by Mn substitution

L.H. Jin[a,*], J.Z. Lu[a], D.P. Song[b], B.B. Yang[c,d], X.B. Zhu[c,d]

[a] State Key Laboratory of Disaster Prevention and Reduction for Power Grid Transmission and Distribution Equipment, State Grid Hunan Electric Power Corporation Disaster Prevention and Reduction Center, Changsha 410007, People's Republic of China
[b] Department of Physics, Jiangsu University of Science and Technology, Zhenjiang 212003, People's Republic of China
[c] Key Laboratory of Materials Physics, Institute of Solid State Physics, Chinese Academy of Sciences, Hefei 230031, People's Republic of China
[d] University of Science and Technology of China, Hefei 230026, People's Republic of China

ARTICLE INFO

Keywords:
Chemical solution deposition
Thin films
Mn substitution
Ferroelectric properties

ABSTRACT

The effect of Mn substitution on microstructure and electrical properties of epitaxial $BiFeO_3$ (BFO) thin films grown by an all-solution approach was investigated. Raman analysis reveals that the Mn atoms substitution at Fe sites can result in Jahn-Teller distortion and thus lead to the weakness of long-range ferroelectric order. In addition, the break-down characteristics of BFO thin films are improved with the increase of Mn atoms content, although the leakage current is gradually increased. Meanwhile, the grain size, the dielectric constant and loss are also increased with the increase of Mn content. The *P-E* hysteresis loops and PUND results demonstrate that the intrinsic ferroelectric polarization is effectively improved with Mn atoms substitution as the grain size increased and Mn atoms play a role of nucleation sites. However, the ferroelectric properties are deteriorated with the excess substituted Mn content due to the higher leakage current.

1. Introduction

Multiferroic thin films are expanding a new dimension to peculiar fundamental physical phenomena as well as industrial applications, such as piezoelectric micro-electromechanical systems (MEMS), memories and the next generation spintronic devices [1–4]. During the past few years, many growth techniques were used to fabricate multiferroic thin films, especially $BiFeO_3$ (BFO) thin film, including pulse laser deposition (PLD), metal-organic chemical vapor deposition (MOCVD), off-axis radio-frequency magnetron sputtering (RF), molecular beam epitaxy (MBE), atomic layer deposition (ALD) and chemical solution deposition (CSD) [5–10]. It is necessary to select a most appropriate technique for BFO thin films. The CSD technique as a cost-effective and easy scale-up manufacturing method for large-area thin film preparation could be one of the optimal choices for commercial application [11].

However, ferroelectric properties of the CSD derived BFO thin films are limited by lower breakdown field [12]. In order to overcome the shortcomings, the site engineering, as a flexible method, has been used to improve the ferroelectric properties of BFO thin films [13]. Generally, ion substitutions for A site and/or B site are used to modify the properties of BFO thin films. Substitution of Bi^{3+} ions on A site, replaced by other ions, can influence the Bi $6s^2$ lone pair, Bi volatile and the lattice structure. Substitution of Fe^{3+} ions on B site, replaced by other transition metal ions, can impact the d shell configuration and suppression of Fe valence change. Thus, it will modify the electronic band and lattice structures, and then tune the ferroelectric properties of BFO thin films in the way of ion substitution.

Transition metal Mn substituted at Fe site is often used to reduce the leakage current and tune the magnetism [13–15]. The previous works of CSD derived BFO thin film and Mn-substituted BFO thin films mainly focused on polycrystalline thin films, while the BFO parents exhibited poor ferroelectric properties with unsaturated *P-E* loops [16–20]. Generally, leakage current plays a determinate role for the improvement of ferroelectricity in ferroelectric films [21]. For CSD derived Mn-substituted BFO thin films, the opposite trends of leakage current with Mn substitution have been reported. For example, Singh et al. showed that the leakage current density steadily increased with the increase of the Mn content, which suggested that the better breakdown characteristics lead to the well-saturated *P-E* loop [12]. On the contrary, Liu et al. observed that the substitution of Mn atoms can give rise to lower leakage current, accompanied with the improved ferroelectric properties [14]. To address the above controversy and explore the effects of Mn substitution at Fe site in BFO thin films, it is vital to examine the results in epitaxial grown films.

In this paper, the epitaxial $BiFe_{1-x}Mn_xO_3$ (BFMs) thin films with

* Corresponding author.
E-mail address: jinlh@mail.ustc.edu.cn (L.H. Jin).

https://doi.org/10.1016/j.ceramint.2018.03.241
Received 5 January 2018; Received in revised form 27 March 2018; Accepted 27 March 2018
Available online 30 March 2018

thickness about 300 nm were grown by CSD method on solution-route deposited $SrRuO_3$ (SRO) bottom electrodes buffered single crystal $LaAlO_3$ (LAO) substrates. The effects of Mn substitution on the microstructure, dielectric, leakage and ferroelectric properties of BFO thin films were investigated, and the results provide a sight of tuning the electricalsight properties of Mn-substituted epitaxial BFO thin films prepared by CSD route.

2. Experiment

The SRO bottom electrodes were firstly deposited onto LAO(001) single crystal substrates by the CSD processing with the annealing temperature of 700 °C in air as which had been reported in our previous work [22]. The derived SRO bottom electrodes are epitaxial thin films with room-temperature resistivity with a magnitude of 10^{-4} Ω cm. Subsequently, the stoichiometric $BiFe_{1-x}Mn_xO_3$ precursor solutions (x = 0, 0.03, 0.07, 0.10, 0.15) were spin coated on the SRO buffered LAO substrates to form wet $BiFe_{1-x}Mn_xO_3$ thin films, followed by pyrolyzed at 350 °C for 10 min and annealed at 500 °C for 30 min in air. Finally, the obtained thin films with x = 0, 0.03, 0.07, 0.10, 0.15 are defined as BFM0, BFM3, BFM7, BFM10, BFM15 for simplicity. Here, the $BiFe_{1-x}Mn_xO_3$ precursor solutions were prepared from propionic acid (PPA) based solution. The bismuth acetate, iron acetate and manganese acetate were used as starting materials, and PPA as the solvent. Ethanolamine was added to stabilize the solutions, and excess of 5 mol% bismuth acetate was used to compensate the Bi loss during the annealing process.

X-ray diffraction with a monochromatic Cu-K_α radiation (Philips X'pert Pro) was used to check up the crystal phase and the crystalline quality. The room-temperature polarized Raman measurements were carried out in the range of 100–670 cm^{-1} using micro-Raman spectroscopy (T64000, Horlba Jobin Yvon). Atomic force microscopy (AFM, CYPHER ES) was used to detect the surface morphology. The chemical states were analysed by an X-ray photoelectron spectroscopy (XPS, ESCALAB250Xi, Thermo). Circular Au top electrodes with a diameter of 0.1 mm were sputtered onto the film surfaces by ion sputtering (JS-1600, Hetong Co., Ltd) through a shadow mask for electrical measurements. The room-temperature dielectric responses were investigated by using a precision inductance, capacitance, and resistance meter (TH2828/A/S, Tonghui Electronic Co., Ltd). The leakage and ferroelectric properties were measured by a standardized ferroelectric test system (Precision Premier Π, Radiant Technologies).

3. Results and discussion

Fig. 1(a) shows the XRD patterns of all BFMs thin films on SRO buffered LAO(001) substrates. All the films are crystallized and with no detectable secondary phases. Moreover, the derived BFMs thin films show epitaxy grain growth along (001) orientation with the Lotgering factor of 1. To further confirm the epitaxy, the ϕ-scanning measurements are carried out. The partial results are exhibited in Fig. 1(b) and (c) for the thin films BFM0 and BFM7 respectively. Clearly, four sharp ϕ-scanning peaks 90° apart of the BFMs (110), the SRO (110) and the LAO (110) indicate the 4-fold symmetry of cubic BFMs thin films on cubic SRO/LAO substrate. The heteroepitaxial relationship among BFMs, SRO and LAO can be derived as (001)BFMs//(001)SRO//(001) LAO and [110]BFMs//[110]SRO//[110]LAO.

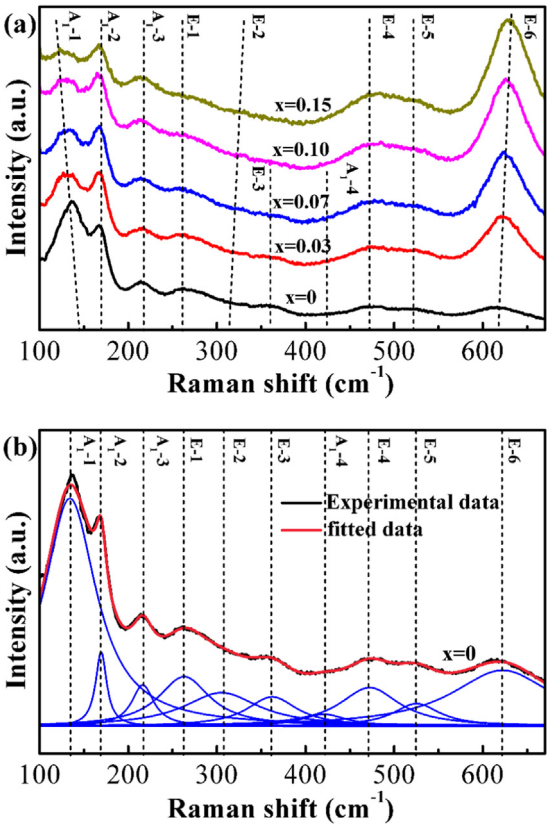

Fig. 2. (a) Room-temperature Raman spectra of all BFMs thin films. (b) The fitted Raman spectra of the BFO thin film.

Fig. 2(a) shows the room-temperature Raman spectra of the BFMs thin films on SRO/LAO(001) single crystal substrates within the frequency range of 100–670 cm^{-1}. All the measured spectra of BFMs thin films were fitted and decomposed into Gaussian components. As a typical result, the fitted Raman spectrum of the BFM0 is displayed in Fig. 2(b). The frequency of each Raman active mode is listed in Table 1. Obviously, the A_1 and E-symmetry normal modes are in agreement with the Raman active vibration modes of the $R3c$ space group based on the

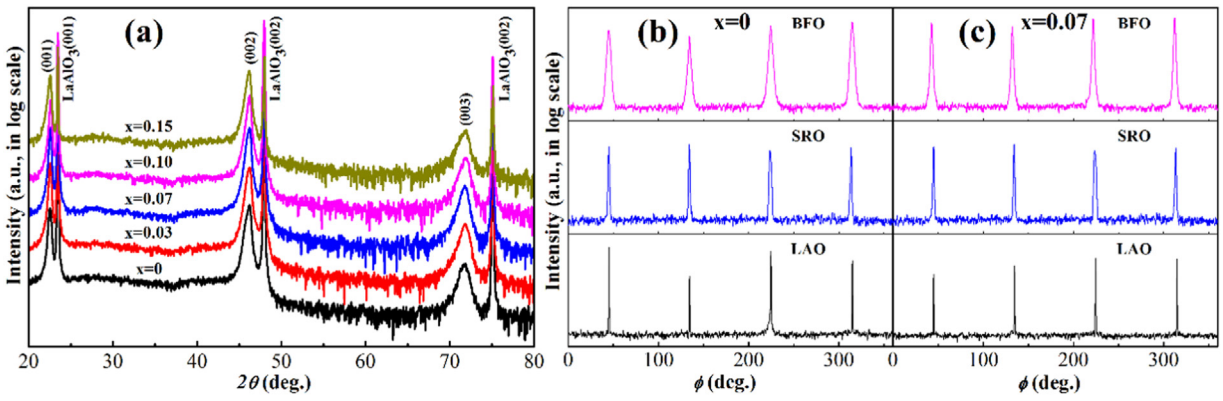

Fig. 1. (a) XRD patterns of all the BFMs thin films. (b) and (c) ϕ-scans of (110) reflections of BFO, SRO and LAO for the thin films BFM0 and BFM7 respectively.

Table 1
Raman modes of the $BiFe_{1-x}Mn_xO_3$ thin films.

Raman active modes (cm^{-1})	x = 0	x = 0.03	x = 0.07	x = 0.1	x = 0.15
A_1	134	128	127	121	115
A_1	169	168	168	168	168
A_1	216	215	216	216	217
E-1	263	262	262	263	265
E-2	305	319	335	345	341
E-3	362	366	371	–	–
A_1	421	420	420	–	–
E-4	472	475	476	476	477
E-5	525	530	532	531	532
E-6	622	625	626	628	631

$13(4A_1+9E)$ Raman-active modes. The change in peak position and intensity was observed with the increase of Mn content. It can be observed that the Raman modes A_1 shift toward lower frequency (134–115 cm^{-1}) and the corresponding intensity decreases with the increase of Mn content. The obtained results indicate that there is a change of Bi–O covalent bonds as a result of the decline in the stereochemical activity of the Bi lone electron pair and thus in long range ferroelectric order, which will reduce ferroelectric behavior of BFO thin films [23]. In addition, with the increase of Mn content from 0% to 15%, continuous shift towards higher wave-number is observed in both Raman modes *E*-4 and *E*-6 from 472 cm^{-1} to 477 cm^{-1} and 622 cm^{-1} to 631 cm^{-1}, respectively. Moreover, the intensity of Raman peaks increase with the increase of Mn content. It is well known that high-frequency Raman phonon modes are strongly dominated by vibrational and rotational motion of FeO_6 octahedra [24]. The increase in intensity of *E*-4 and *E*-6 should be attributed to the stretching and bending of MnO_6 octahedra, which result in Jahn-Teller distortion [25]. Meanwhile, the observed shift in *E*-6 mode should be attributed to the change of force constant and ionic mass for the substitutive Mn elements. As is well known, the frequency of phonon mode is proportional to $(k/M)^{1/2}$, where k is the force constant related to bond strength and ionic radius of the constituent ions and M is the reduced mass of the mode [24]. Since the radius and mass of Mn^{3+} ion are smaller than that of Fe^{3+} ion, the frequency of *E*-4 and *E*-6 modes is shifted to the high frequency with the increase of Mn substitution. The changes in peak intensity and position indicate structural distortion due to the Mn substitution, and it suggests that the Mn substitution in BFO thin films will degrade the ferroelectric behavior.

The surface morphology of thin films was investigated by using AFM. Fig. 3(a)–(e) show the surface morphologies of BFMs thin films in measurement area of $3 \times 3\,\mu m^2$. As seen in Fig. 3, the grain size is gradually increased with the increase of Mn content. In addition, the root mean square (rms) value of the surface roughness of BFM0, BFM3, BFM7, BFM10 and BFM15 is approximately 4.7, 3.8, 3.7, 4.2 and 4.9 nm, respectively, which is smaller than that of others' reports [16,26]. It is decreased before the BFM7 and then increased with the Mn content increased. The BFM7 has the smallest rms value compared to other BFMs thin films, as shown in Fig. 3(f).

Fig. 4(a) shows the leakage current density versus applied electric field (*J-E*) results of all the BFMs thin films measured at room-temperature. The leakage current density of the parent BFO thin film, less than 230 kV/cm, is the lowest in the electric field, but it increases sharply when the electric field exceeds 230 kV/cm. The sharp increase in the current density of the parent BFO thin film will lead to the breakdown behavior rapidly. As a contrast, the sharp increase in the current density does not occur in the Mn-substituted BFO thin films, although the leakage current density steadily increases with the increase of Mn content. The breakdown characteristic of the BFMs thin films is much improved by Mn substitution, which is consistent with previous reports [12,16].

For the leakage current density increased with the increase of Mn content, the theoretical calculation reveals that the electronic structure of the Mn-substituted BFO thin films is significantly modulated comparing with the parent BFO thin films, which will cause an impurity energy level appears in the forbidden band of BFO thin films [27]. On one hand, the impurity energy level is near the Fermi level, so the Mn substitution makes the conversion between Fe^{2+} and Fe^{3+}, and leads to the increased leakage current density. On the other hand, it also could be understood that some Mn atoms replace Fe atoms on B site form a $BiMnO_3$ phase with the same perovskite structure as BFO and a narrower energy band gap [28]. Moreover, the XPS spectra of Fe, O and Mn in BFMs thin films are presented in Fig. S1 and Fig. S2. For Mn-substituted BFO thin films, the number of oxygen vacancies decrease, and the Fe^{2+} ions increase with the increase of Mn substitution. The Mn ions in BFM15 are mainly Mn^{3+}, and the extra of higher valence Mn cations (Mn^{4+}) to Mn-substituted BFO thin films can reduce the number of oxygen vacancies and decrease the Fe ions valence (i.e., transition from Fe^{3+} to Fe^{2+}) for charge compensation [29]. Generally, it is commonly considered that the hopping of electrons from Fe^{2+} to Fe^{3+} acts as an important factor in the electronic conduction in BFO thin films [30]. In addition, the oxygen vacancies are usually considered as the major carriers resulting in the leakage in BFO thin films. Thus, for Mn-substituted BFO thin films, the hopping between Fe^{2+}-Fe^{3+} may dominate the conduction behavior, which results in the increase in leakage current with the increase of Mn content.

As shown in Fig. 4(a), it is observed that no insignificant difference in leakage current between the forward and reverses bias conditions for BFMs thin films. To clarify the conduction mechanism in BFMs thin films, several models have been used to fit the *J-E* curves in positive bias region. Firstly, the space-charge-limited current (SCLC) mechanism was examined. ln*J*-ln*E* characteristics are plotted as shown in Fig. 4(b). In the parent BFO thin film, the plot was divided into three different regions, the fitted slope of each region was 1.20, 1.86 and 18.98. The linear dependence in low electric fields suggests Ohmic contact behavior, while a nearly square law dependence corresponding to a modified Child's law ($J \propto E^2$) in moderate fields demonstrates SCLC conduction mechanism [31]. In higher electric fields, an abrupt increase in leakage with a much higher slope value indicates the trap-filled-limit (TFL) mechanism dominates leakage behavior [32]. In contrast, in Mn-substituted BFO thin films, the plots show linear behaviors over a wide range of the electric field and they obey a power law of $J = CE^n$ (C: constant), the n values are determined to be 1.50, 1.92, 1.63 and 1.85 for the samples with x = 0.03, 0.07, 0.10 and 0.15, respectively. Therefore, the leakage current at high electric fields can be increased slightly in Mn-substituted BFO thin films. The second mechanism is bulk-limited Poole-Frenkel emission (PF emission), which involves the consecutive hopping of charges between defect trap centers [33]. PF emission mechanism can be investigated by plotting the leakage data as log*J*/*E* vs log$E^{1/2}$(not shown here), the results indicating that PF emission is not in operation in these thin films. The third mechanism is interface-limited Schottky emission, which is related to the difference of Femi-level between metal electrode and ferroelectric thin film [33], as shown in Fig. 4(c). To identify whether Schottky emission dominates the leakage behavior, it is necessary to extract the optical permittivity *K* value coinciding with the intrinsic material properties. The index of refraction for BFO is known to be n = 2.5, thus an optical permittivity $K = n^2 = 6.25$ is expected. From the Schottky plot of Fig. 4(c), a *K* value for BFMs thin films is consistent to the ideal optical dielectric permittivity, indicating that the leakage behavior in BFMs thin films are dominated by the Schottky emission. That is to say, the Metal-Ferroelectric contact is a rectifying (Schottky) contact. However, the leakage mechanism in the BFM0 at higher electric fields is dominated by the interface-limited Fowler-Nordheim (FN) tunneling conduction mechanism, caused by the injection of carriers into a ferroelectric layer from electrode with tunneling through an interfacial energy barrier [32], as shown in Fig. 4(d), which suggests that the breakdown field of the BFO thin film is lower than that of Mn-substituted BFO thin films.

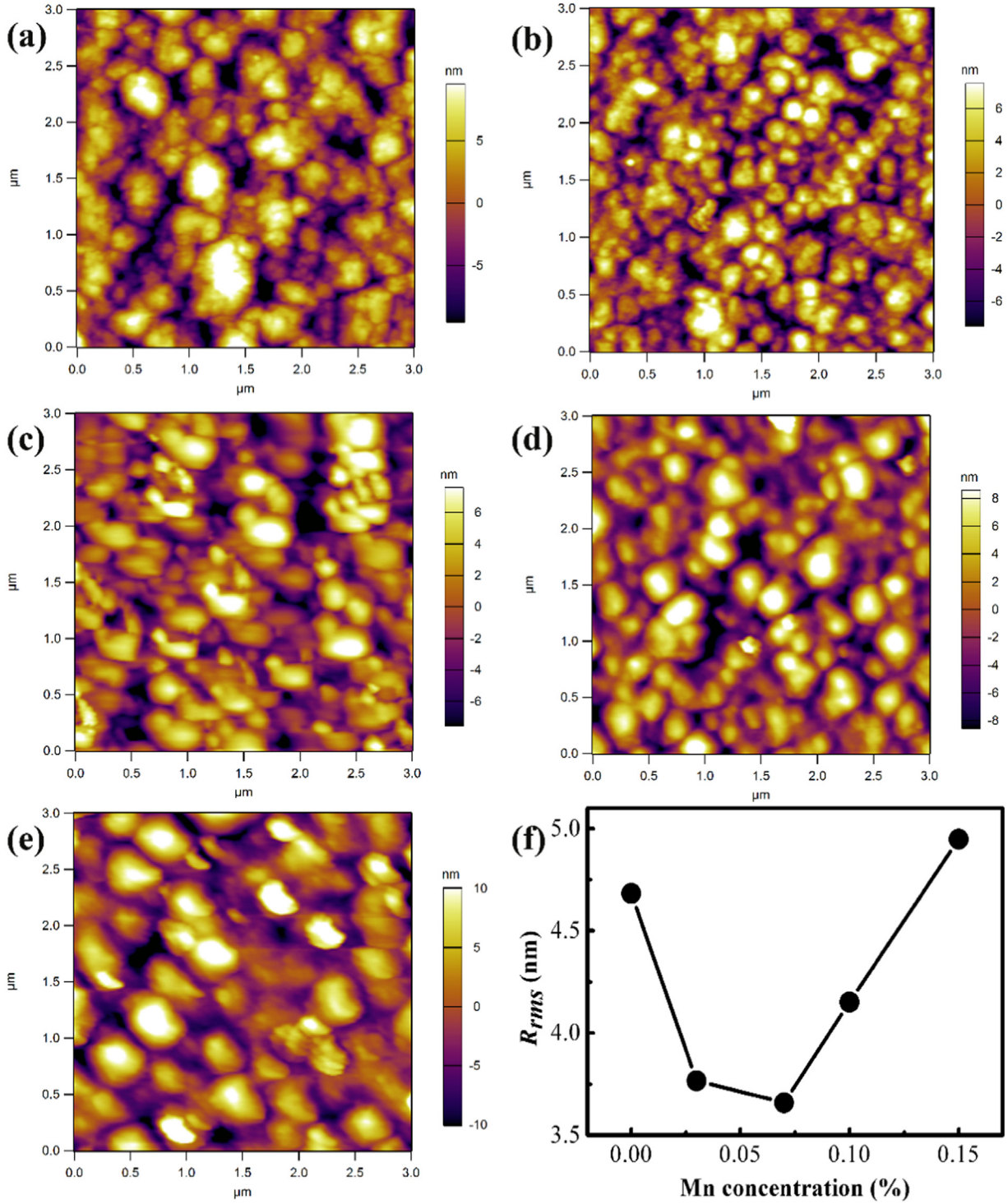

Fig. 3. AFM images of $BiFe_{1-x}Mn_xO_3$ thin films, (a)-(e) for x = 0, 0.03, 0.07, 0.1, 0.15, respectively. (f) The root mean square value of the surface roughness of the sample increases with the increase of Mn content.

The room-temperature frequency dependent dielectric constant ε_r results of all BFMs thin films are shown in Fig. 5(a). The dielectric constant ε_r of all BFMs thin films exhibits maximum values at the lowest frequency, and monotonously increases as the Mn content increases. Meanwhile, the dielectric constant ε_r decreases more rapidly with the increase of the frequency in low test range of higher Mn content BFMs thin films. This phenomenon can be attributed to the dipole orientation polarization formed by more space charge defects under external electric fields [19]. As the frequency increases, the dielectric constant gradually decreases and tends to be a constant value, which arises from the fact that the response of polarization formed by space charge defects to the applied field cannot occur instantaneously [10]. It can be seen that the dielectric constant increases as the Mn content increases and the respective ε_r values at 1 MHz is 157.6, 175.9, 180.0, 189.6 and 193.9. It is well known that the increase of grain size can lead to an increase in dielectric constant [10], so the dielectric constant increases with the increase of the Mn content. In addition, the dielectric constant of $BiMnO_3$ thin films can reach 1400, so the formation of $BiMnO_3$ phase

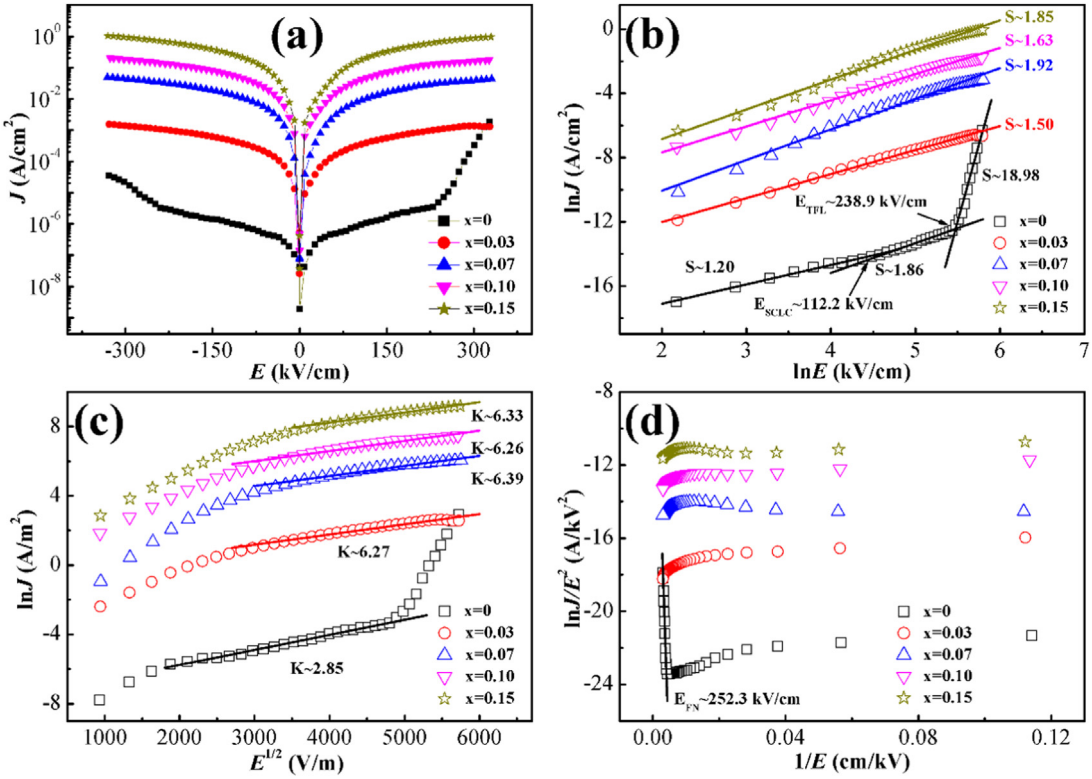

Fig. 4. (a) Leakage current density versus applied field (*J-E* curves) for all BFMs thin films. Leakage current density fitted by (b) SCLC, (c) Schottky emission and (d) FN tunneling for the BFMs thin films.

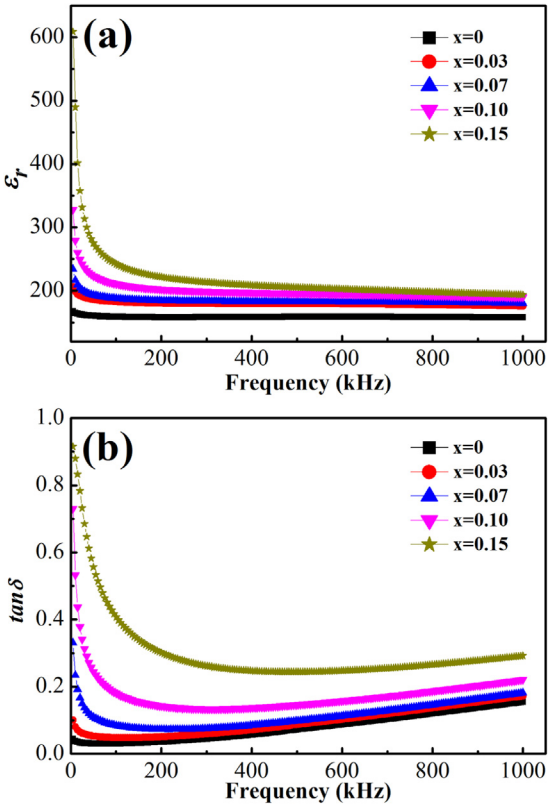

Fig. 5. Frequency dependent room-temperature (a) dielectric constant and (b) dielectric loss of all BFMs thin films.

as the same perovskite structure with $BiFeO_3$ by Fe-site substitution with Mn atoms will lead to the increase of dielectric constant for BFMs thin films [34].

Fig. 5(b) exhibits the frequency dependent room-temperature dielectric loss tan δ, which shows the same trend as ε_r with the increase of the Mn content in low test frequency, while the corresponding tan δ value at 1 MHz is 0.154, 0.172, 0.182, 0.221 and 0.292 for $BiFe_{1-x}Mn_xO_3$ thin films with x = 0, 0.03, 0.07, 0.10 and 0.15, respectively. It is well known that the total contribution to tan δ is the sum of conduction loss due to free vacancies and dipolar Debye loss, which can be described as $\tan\delta = 4\pi\sigma/\omega\varepsilon_r + (\varepsilon_s - \varepsilon_\infty)\,\omega\tau/(\varepsilon_s + \varepsilon_\infty\omega^2\tau^2)$, where σ is the electrical conductivity, ω is the frequency, ε_r is the measured dielectric constant, ε_s is the static or the low frequency dielectric constant and ε_∞ is the high frequency dielectric constant [35]. According to the formula, it can be concluded that the first term is the predominant factor and the conductivity is the dominant contribution for the tan δ at low frequency. So the higher leakage current could lead to bigger tan δ at low frequency. The second term becomes dominant and the relaxation effects play important roles in the determination of tan δ within higher frequency. The loss may be derived from the dipolar impurities or dipoles come from defects due to Fe-site substitution with Mn atoms. In addition, the increase in tan δ with frequency at high test frequency is owing to that the charge carries in the film do not have time to respond to the external electric field and the maximum electrical energy is transferred to the oscillation ions.

In order to properly understand the polarization behavior of BFMs thin films, two various polarization measurement techniques have been used to investigate it. The *P-E* hysteresis loop and pulsed polarization positive-up negative-down (PUND) measurement results are shown in the Fig. 6(a) and (b). Fig. 6(a) shows the *P-E* hysteresis loops of BFMs thin films measured at 20 kHz and room-temperature. The BFMs thin films with x = 0, 0.03, 0.07 and 0.10 show well-saturated rectangular *P-E* loops with P_r values of 46, 53, 71 and 61 μC/cm^2, respectively, as the leakage current density is below 2×10^{-1} A/cm^2 at 300 kV/cm.

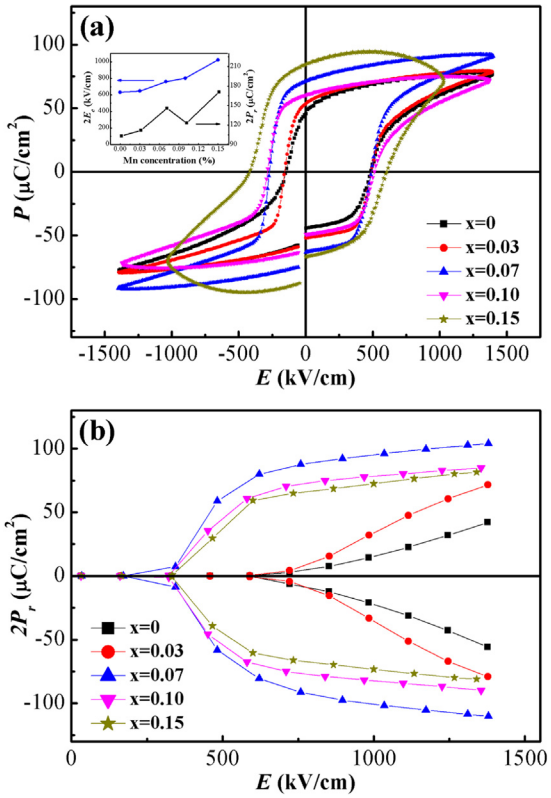

Fig. 6. (a) Polarization behavior of all BFMs thin films, measured by *P-E* hysteresis loops at 20 kHz, the inset shows the characteristics of $2P_r$ and $2E_c$ versus Mn content. (b) Polarizations measured by PUND for all BFMs thin films.

The *P-E* hysteresis loop shows better rectangularity with the increase of Mn content. The higher P_r value for the thin film BFM15 with lossy loop behavior may be due to its largest leakage current density of the order of 1 A/cm^2 at 300 kV/cm compared with other films. Although the leakage current density is the lowest, the rectangularity is the poorest and the $2P_r$ is the smallest for the thin film BFM0. On the other hand, the increased grain size could facilitate the motion of domain walls and the reversal of domain due to the decrease in grain boundaries in Mn-substituted thin films, which will facilitate the domain switching and result in a higher value of P_r [21]. In addition, the substituted Mn atoms may act as nuclei in domain switching [36].

It is well known that the conventional *P-E* loop measurement can be strongly influenced by the leakage behavior [21], so as to have a consideration on the contribution of leakage current towards the overall polarization, the PUND measurement is carried out at room-temperature. The corresponding results are shown in Fig. 6(b). It can be seen that for all BFMs thin films, the respective $2P_r$ value is 39, 68, 103, 84 and 81 μC/cm^2, which are smaller than the polarization measured by *P-E* hysteresis loop measurement, also smaller than the theoretical value of 120 μC/cm^2 of (001)-oriented BFO thin film. In addition, with the increase of Mn content, the $2P_r$ value increases firstly and then decreases for BFMs thin films, while the thin film BFM7 has the maximum $2P_r$ value.

From the results of *P-E* and PUND measurements, it can be deduced that the substitution of Mn atoms at Fe site can affect the ferroelectric properties of the BFO thin film. Combined with the results of both Raman and AFM, it can be deduced that with the substitution of Mn atoms at Fe site, the Jahn-Teller distortion of BFMs thin film has a continuous change of Bi–O covalent bonds as a result of the decline in the stereo-chemical activity of the Bi lone electron pair and thus in long-range ferroelectric order. However, the substitution of Mn atoms at Fe site can lead to the increase in grain size, which will decrease the clamping effect and lead to a bigger value of $2P_r$. Moreover, the Mn atoms may play a role of nucleation sites, which makes the ferroelectric domain easier to switch and result in the increase in polarization of the BFMs thin films. Thus the above inverse effects caused by the substitution with Mn atoms will lead to the results of PUND measurement of BFMs thin films.

4. Conclusions

In summary, an all-solution processing has been successfully used to deposit epitaxial BFMs/$SrRuO_3$/$LaAlO_3$ thin films. XRD and Raman results reveal that the obtained films are (001) epitaxial with a distorted rhombohedral structure of *R3c* symmetry accompanied with Jahn-Teller distortion. Substitution of Fe-site with Mn atoms can effectively improve the break-down characteristics of BFO thin films, although the leakage current gradually increases with the increase of Mn content in thin films. Meanwhile, the electrical transport mechanism is also changed with Mn substitution. For the thin film BFM0, the leakage at low electric fields can be described by the Ohmic behavior, while the Fowler-Nordheim tunneling behavior is applicable at high electric fields. In the case of Mn atoms substitution, the interface between the electrode and the thin film with Schottky contact controls the charge injection, and results in the Schottky barrier domination in conduction. Moreover, the ferroelectric properties of BFMs thin films are effectively improved, which can be attributed to the increased grain sizes of BFMs thin films and that Mn atoms play a role of nucleation sites with Mn substitution.

Acknowledgements

This study was supported by the National Basic Research Program of China (2014CB931704), the National Nature Science Foundation of China under Contract no. U1432137, 11204316, 11374304, U1232210 and 11274313, and by the Users with Potential Foundation (2015HSC-UP004) from Hefei Science Center, CAS. The authors acknowledge Dr. Ranran Zhang for Raman, Dr. Weike Wang for XPS and Dr. Dapeng Cui for AFM measurements.

Appendix A. Supplementary material

Supplementary data associated with this article can be found in the online version at http://dx.doi.org/10.1016/j.ceramint.2018.03.241.

References

[1] G. Catalan, J.F. Scott, Physics and applications of bismuth ferrite, Adv. Mater. 21 (2009) 2463–2485.
[2] R.J. Zeches, M.D. Rossell, J.X. Zhang, A.J. Hatt, Q. He, C.H. Yang, A. Kumar, C.H. Wang, A. Melville, C. Adamo, G. Sheng, Y.H. Chu, J.F. Ihlefeld, R. Erni, C. Ederer, V. Gopalan, L.Q. Chen, D.G. Schlom, N.A. Spaldin, L.W. Martin, R. Ramesh, A strain-driven morphotropic phase boundary in $BiFeO_3$, Science 326 (2009) 977–980.
[3] R. Ramesh, N.A. Spaldin, Multiferroics: progress and prospects in thin films, Nat. Mater. 6 (2007) 21–29.
[4] D. Sando, A. Barthélémy, M. Bibes, $BiFeO_3$ epitaxial thin films and devices: past, present and future, J. Phys.: Condens. Matter 26 (2014) 473201.
[5] J. Wang, J.B. Neaton, H. Zheng, V. Nagarajan, S.B. Ogale, B. Liu, D. Viehland, V. Vaithyanathan, D.G. Schlom, U.V. Waghmare, N.A. Spaldin, K.M. Rabe, M. Wuttig, R. Ramesh, Epitaxial $BiFeO_3$ multiferroic thin film heterostructures, Science 299 (2003) 1719–1722.
[6] S.Y. Yang, F. Zavaliche, L. Mohaddes-Ardabili, Metalorganic chemical vapor deposition of lead-free ferroelectric $BiFeO_3$ films for memory applications, Appl. Phys. Lett. 87 (2005) 102903.
[7] J.G. Wu, J. Wang, $BiFeO_3$ thin films of (111)-orientation deposited on $SrRuO_3$ buffered Pt/TiO_2/SiO_2/Si(100) substrates, Acta Mater. 58 (2010) 1688–1697.
[8] J.F. Ihlefeld, W. Tian, Z.K. Liu, W.A. Doolittle, M. Bernhagen, P. Reiche, R. Uecker, R. Ramesh, D.G. Schlom, Adsorption-controlled growth of $BiFeO_3$ by MBE and integration with wide band gap semiconductors, IEEE Trans. Ultrason. Ferroelectr. Frequency Control 56 (2009) 1528–1533.
[9] B. Marchand, P. Jalkanen, V. Tuboltsev, M. Vehkamäki, M. Puttaswamy, M. Kemell, K. Mizohata, T. Hatanpää, A. Savin, J. Räisänen, M. Ritala, M. Leskelä, Electric and magnetic properties of ALD-grown $BiFeO_3$ films, J. Phys. Chem. C. 120 (2016) 7313–7322.

[10] L.H. Jin, X.W. Tang, R.H. Wei, B.B. Yang, J. Yang, W.H. Song, J.M. Dai, X.B. Zhu, Y.P. Sun, $BiFeO_3$(00l)/$LaNiO_3$/Si thin films with enhanced polarization: an all-solution approach, Rsc Adv. 6 (2016) 78629–78635.
[11] G. Subramanyam, M.W. Cole, N.X. Sun, T.S. Kalkur, N.M. Sbrockey, G.S. Tompa, X.M. Guo, C.L. Chen, S.P. Alpay, G.A. Rossetti Jr., K. Dayal, L.Q. Chen, D.G. Schlom, Challenges and opportunities for multi-functional oxide thin films for voltage tunable radio frequency/microwave components, J. Appl. Phys. 114 (2013) 191301.
[12] S.K. Singh, H. Ishiwara, K. Maruyama, Room temperature ferroelectric properties of Mn-substituted $BiFeO_3$ thin films deposited on Pt electrodes using chemical solution deposition, Appl. Phys. Lett. 88 (2006) 262908.
[13] C.H. Yang, D. Kan, I. Takeuchi, V. Nagarajand, J. Seidel, Doping $BiFeO_3$: approaches and enhanced functionality, Phys. Chem. Chem. Phys. 14 (2012) 15953–15962.
[14] W.L. Liu, G.Q. Tan, G.H. Dong, X. Yan, W. Ye, H.J. Ren, A. Xia, Structure transition and multiferroic properties of Mn-doped $BiFeO_3$ thin films, J. Mater. Sci: Mater. Electron 25 (2014) 723–729.
[15] S. Gupta, M. Tomar, V. Gupta, Raman spectroscopy of nanocrystalline Mn-doped $BiFeO_3$ thin films, J. Exp. Nanosci. 8 (2013) 261–266.
[16] S.K. Singh, H. Ishiwara, K. Sato, K. Maruyama, Microstructure and frequency dependent electrical properties of Mn-substituted $BiFeO_3$ thin films, J. Appl. Phys. 102 (2007) 094109.
[17] J.Z. Huang, Y. Wang, Y.H. Lin, M. Li, C.W. Nan, Effect of Mn doping on electric and magnetic properties of $BiFeO_3$ thin films by chemical solution deposition, J. Appl. Phys. 106 (2009) 063911.
[18] Y.J. Ren, X.H. Zhu, J.L. Zhu, J.G. Zhu, D.Q. Xiao, Comparative study of Mn^{3+} and Mn^{2+} doping effects on structure and electrical properties of $BiFeO_3$ thin films, Ceram. Int 41 (2015) S234–S239.
[19] Y.J. Ren, X.H. Zhu, C.Y. Zhang, J.L. Zhu, J.G. Zhu, D.Q. Xiao, Saturated hysteresis loops and conduction mechanisms in Mn-doped $BiFeO_3$ thin films derived from sol–gel process, J. Mater. Sci: Mater. Electron 26 (2015) 1719–1726.
[20] K. Singh, S.K. Singh, D. Kaur, Tunable multiferroic properties of Mn substituted $BiFeO_3$ thin films, Ceram. Int 42 (2016) 13432–13441.
[21] L. Jin, F. Li, S.J. Zhang, Decoding the fingerprint of ferroelectric loops: comprehension of the material properties and structures, J. Am. Ceram. Soc. 97 (2014) 1–27.
[22] D.Y. Yang, X.W. Tang, R.H. Wei, Z.Z. Hui, W.H. Song, X.B. Zhu, Y.P. Sun, Epitaxial growth of $SrRuO_3$ thin films with different orientation by chemical solution deposition, J. Alloy. Compd. 682 (2016) 154–159.
[23] G.L. Yuan, S.W. Or, H.L.W. Chan, Raman scattering spectra and ferroelectric properties of $Bi_{1-x}Nd_xFeO_3$ (x = 0-0.2) multiferroic ceramics, J. Appl. Phys. 101 (2007) 064101.
[24] S. Gupta, M. Tomar, V. Gupta, Study on Mn-induced Jahn–Teller distortion in $BiFeO_3$ thin films, J. Mater. Sci. 49 (2014) 5997–6006.
[25] D. Do, J.W. Kim, S.S. Kim, Effects of Dy and Mn codoping on ferroelectric properties of $BiFeO_3$ thin films, J. Am. Ceram. Soc. 94 (2011) 2792–2795.
[26] Z. Wen, G.D. Hu, S.H. Fan, C.H. Yang, W.B. Wu, Y. Zhou, X.M. Chen, S.G. Cui, Effects of annealing process and Mn substitution on structure and ferroelectric properties of $BiFeO_3$ films, Thin Solid Films 517 (2009) 4497–4501.
[27] G.Y. Chen, G.F. Bi, L. Song, Y.K. Weng, D.F. Pan, Y.C. Li, S. Dong, T. Tang, J.M. Liu, J.G. Wan, Magnetization switching in the $BiFe_{0.9}Mn_{0.1}O_3$ thin films modulated by resistive switching process, Appl. Phys. Lett. 109 (2016) 112903.
[28] J.H. Kim, H. Funakubo, Y. Sugiyama, H. Ishiwara, Characteristics of undoped and Mn-doped $BiFeO_3$ films formed on Pt and $SrRuO_3$/Pt electrodes by radio-frequency sputtering, Jpn. J. Appl. Phys. 48 (2009) 09KB02.
[29] H.J. Lee, M.H. Park, Y.J. Kim, C.S. Hwang, J.H. Kim, H. Funakubo, H. Ishiwara, Improved ferroelectric property of very thin Mn-doped $BiFeO_3$ films by an inlaid Al_2O_3 tunnel switch, J. Appl. Phys. 110 (2011) 074111.
[30] Q.Q. Ke, X.J. Lou, Y. Wang, J. Wang, Oxygen-vacancy-related relaxation and scaling behaviors of $Bi_{0.9}La_{0.1}Fe_{0.98}Mg_{0.02}O_3$ ferroelectric thin films, Phys. Rev. B 82 (2010) 024102.
[31] J.G. Wu, J. Wang, D.Q. Xiao, J.G. Zhu, Leakage mechanism of cation-modified $BiFeO_3$ thin film, AIP Adv. 1 (2011) 022138.
[32] X.W. Tang, X.B. Zhu, J.M. Dai, Y.P. Sun, Self-limited grain growth, dielectric, leakage and ferroelectric properties of nanocrystalline $BiFeO_3$ thin films by chemical solution deposition, Acta Mater. 61 (2013) 1739–1747.
[33] G.W. Pabst, L.W. Martin, Y.H. Chu, R. Ramesh, Leakage mechanisms in $BiFeO_3$ thin films, Appl. Phys. Lett. 90 (2007) 072902.
[34] W. Eerenstein, F.D. Morrison, J.F. Scott, N.D. Mathur, Growth of highly resistive $BiMnO_3$ films, Appl. Phys. Lett. 87 (2005) 101906.
[35] D.B. Sirdeshmukh, L. Sirdeshmukh, K.G. Subhadra, Micro- and Macro-Properties of Solids, Springer-Verlag, Berlin Heidelberg, Germany, 2006.
[36] Y. Yoneda, Y. Kitanaka, Y. Noguchi, M. Miyayama, Electronic and local structures of Mn-doped $BiFeO_3$ crystals, Phys. Rev. B 86 (2012) 184112.